ELSEVIER

Journal of Nuclear Materials 290–293 (2001) 798–804

journal of nuclear materials

www.elsevier.nl/locate/jnucmat

Section 7. Control of plasma boundary, e.g., by divertors, pumping and biasing

Control of divertor geometry and performance of the ergodic divertor of Tore Supra

Ph. Ghendrih [a,*], M. Bécoulet [a], L. Costanzo [a], Y. Corre [a], C. Grisolia [a], A. Grosman [a], R. Guirlet [a], J. Gunn [a], T. Loarer [a], P. Monier-Garbet [a], G. Mank [b], R. Reichle [a], J.-C. Vallet [a], M. Zabiégo [a], A. Azéroual [a], J. Bucalossi [a], P. Devynck [a], C De Michelis [a], K.H. Finken [b], J. Hogan [c], F. Laugier [a], F. Nguyen [a], B. Pégourié [a], F. Saint-Laurent [a], B. Schunke [a], Tore Supra Team

[a] *Association Euratom-CEA sur la fusion, CEA Cadarache, F-13108 St Paul lez Durance cedex, France*
[b] *Institut für Plasmaphysik, Forschungszentrum Jülich, Association EURATOM-KFA, D-52425 Jülich, Germany*
[c] *Oak Ridge National Laboratory, Oak Ridge, TN, USA*

Abstract

Experimental evidence of the location of the ergodic divertor separatrix is shown to agree with the predicted value given by codes. Variation of this position modifies the divertor tightness, defined as the ratio of the divertor to core density. This effect is governed by laminar transport, i.e., transport proportional to the magnitude of the perturbation. Operation with feedback control of the divertor temperature allows one to optimise the choice of injected impurity species. At 10 eV divertor temperature, nitrogen is shown to lead to the largest decrease in energy flux to the divertor at lowest contribution to Z_{eff}. Parallel energy fluxes as low as 2 MW m^{-2} are thus achieved on the target plates. For this impurity, radiation is localised in the divertor volume thus leading to radiation compression close to 10. The ergodic divertor appears as a powerful tool to control plasma–wall interaction with no loss of core confinement or plasma current.

Keywords: Divertor; Ergodic divertor

1. Introduction

Despite ongoing efforts and progress, the design of an optimised divertor for reactor-grade fusion devices remains a challenge. Part of the difficulty stands in the conflicting performances to be achieved. On the one hand, the divertor must provide the appropriate configuration to generate H-mode confinement while on the other hand it must ensure control of particle recirculation to reduce core contamination and allow for helium ash pumping. Furthermore, the constraint of reducing the energy flux below the technical limitation of actively cooled components must be satisfied. The ergodic divertor represents an alternative solution with an open, poloidally and toroidally symmetric divertor volume. Significant progress has been made in the understanding of this concept [1]. In many aspects, it has been shown that the physics at hand is comparable to that of axisymmetric divertors [2]. Unfortunately, a set of figures of merit, such as the core energy confinement time, is still missing to compare divertor performances. Radiation enhancement with respect to multi-machine scaling [3,4] has been proposed [5]. Helium and impurity compression have also been used. The results presented here are focused on the geometrical means of controlling the configuration. Two figures of merit are introduced. The divertor tightness, ratio of divertor to core density [6], and the radiation compression [7], namely the ratio of the divertor to core impurity concentration, the divertor concentration being measured in terms of radiation

* Corresponding author.
E-mail address: ghendrih@drfc.cad.cea.fr (Ph. Ghendrih).

0022-3115/01/$ - see front matter
PII: S0022-3115(00)00536-5

efficiency. In Section 2, experimental evidence is used to confirm the location of the separatrix as predicted by the codes. The impact of the location of the separatrix on the divertor tightness is analysed in Section 3. Radiation compression within the divertor volume in conjunction with the very low parallel energy fluxes is addressed in Section 4. A summary of the ergodic divertor performances will be found in Section 5.

2. The divertor volume in the ergodic divertor configuration

The divertor geometry is considered as a means of controlling plasma–wall interaction. In the standard axisymmetric divertor configuration, this control is twofold. On the one hand, the magnetic equilibrium and, most important, the separatrix position allow one to channel the energy flux to dedicated high heat flux components, while, on the other hand, the plasma-facing components are organized to increase the closure of the divertor volume. The latter scheme is optimised in terms of neutral confinement and significant success is reported in the control of helium and neon [8]. In the ergodic divertor configuration, no mechanical baffling has been implemented so that the divertor plasma must control particle recirculation. While the X-point is achieved by a major, and hence measurable, perturbation of the poloidal field, $\delta B_\theta \sim B_\theta$, the stochastic boundary of the ergodic divertor is achieved with typically six helical modes of weak magnitude, $\delta B_r \sim 10^{-2} B_\theta$. As a consequence, there is no direct measurement available to characterise the geometry in this configuration.

From the theoretical point of view, the divertor volume being defined by the region of open field lines, one must determine the volume such that the magnetic perturbation is large enough to generate stochastic diffusion of field lines between neighbouring resonances [1]. The ergodic divertor is therefore defined by the spectrum of the magnetic perturbation generated by a specific set of coils. In the case of the Tore Supra ergodic divertor, the poloidal spectrum is rather broad, $m \approx \bar{m} \pm 6$, $\bar{m} = 18$, while the toroidal spectrum is narrower, $n \approx \bar{n} = 6$. Each mode is resonant on a given magnetic surface labelled by $q(r_{m,\bar{n}}) \approx m/\bar{n}$. The magnitude of each mode can be characterised by its island half width, $\delta_i(m,\bar{n}) \propto \sqrt{I_{ED}}$, where I_{ED} is the divertor coil current [1]. The non-linear interaction between neighbouring resonances is evaluated by the Chirikov parameter criterion, $\sigma_{Chirikov} = \delta_{m+1,m}/\Delta_{m+1,m} \geqslant 1$. $\delta_{m+1,m} = \delta_i(m+1,\bar{n}) + \delta_i(m,\bar{n})$ and $\Delta_{m+1,m} = r_{m+1,\bar{n}} - r_{m,\bar{n}}$ are, respectively, the relevant island width and distance between resonant layers. The radial extent over which the Chirikov parameter exceeds unity defines the divertor volume insofar that it actually extends to the wall. For the sake of convenience, the Chirikov parameter is localised at the radius $(r_{m+1,\bar{n}} + r_{m,\bar{n}})/2$ although it characterises the whole volume between the two resonances. This introduces typically a 0.01 m error in the location of the computed separatrix, comparable to that of standard equilibrium reconstruction.

The divertor volume is both poloidally and toroidally symmetric, a major difference with respect to the axisymmetric divertor. Indeed, in the latter configuration only the region from the X-point to the divertor target plate exhibits a sufficient scale to allow for the control of particle influx. Over most of the poloidal circumference, the scrape-off layer (SOL) is very thin, less than 0.01 m. Another consequence of this geometrical feature is to provide a direct match between the plasma volume and the current channel since the SOL stored energy is negligible. In the ergodic divertor configuration, the current channel is restricted to the volume within the separatrix. The SOL extends over more than 0.1 m radially and accounts for more than 30% of the plasma volume. Due to the lack of a measure of the separatrix position, the whole plasma volume is considered, including the significant fraction of open field lines. Therefore, the low confinement volume is included in the confinement analysis. With this definition of the confinement volume, the reference minor radius, a_{ED}, is the radius of the unperturbed magnetic surface tangential to the divertor coil.

Dedicated experiments have been carried out to determine experimentally the location of the separatrix and compare it to the theoretical prediction defined by $\sigma_{Chirikov} = 1$ [9]. In Fig. 1, the theoretical position of the separatrix is plotted in terms of the boundary safety factor q_{edge} (at $\rho = 1$) and of its low field side position, $R_{ext} = \bar{R} + r$, where $\bar{R}$ and r are, respectively, the major and minor radius of the unperturbed magnetic surfaces. During current ramp-up, decreasing q_{edge}, several small regions with $\sigma_{Chirikov} \geqslant 1$ are connected to the wall. They correspond to wings at high poloidal mode number of the sine cardinal-like spectrum of the magnetic perturbation [9]. At $q_{edge} \sim 3.9$, the main stochastic region comes into contact with the wall at $R_{ext} \sim 3.17$ m. The separatrix then steps in over $\Delta R_{ext} \geqslant 0.18$ m as the configuration switches from limiter to divertor configuration. Experimentally, one observes a rise of the energy flux to the divertor target plate and a sharp decrease of iron line emission, Fig. 2, when q_{edge} decreases below 3.9. Pump-out of plasma particles is also observed at this transition [1]. The experimental evidence in Fig. 2 shows that both particle and energy transport respond to the contact of the boundary $\sigma_{Chirikov} = 1$ with the wall. The weak iron emission decreases (by a factor larger than 2) to noise level indicating that metallic impurity screening, energy flux is effectively diverted onto the target plates (rise by a factor of 2). However, these effects weakly depend on the depth of the divertor volume. Indeed, as

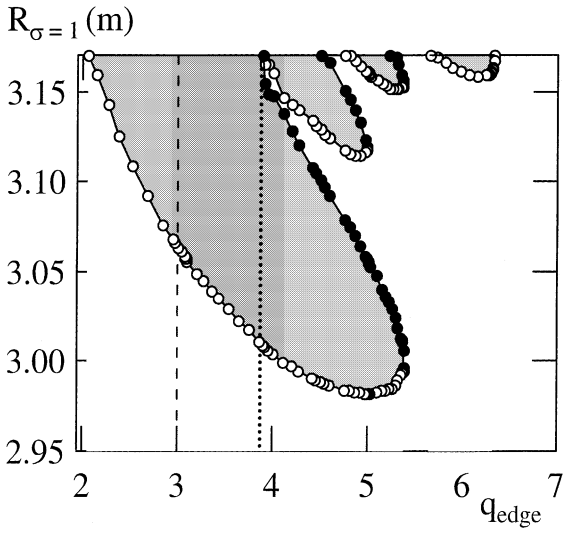

Fig. 1. Radial positions of the separatrix defined by $\sigma_{Chirikov} = 1$ plotted against the edge safety factor q_{edge}. The shaded region is the stochastic region. Transition from limiter to divertor configuration occurs at $q_{edge} \sim 3.9$, dotted line and optimum configuration is at $q_{edge} \sim 3$.

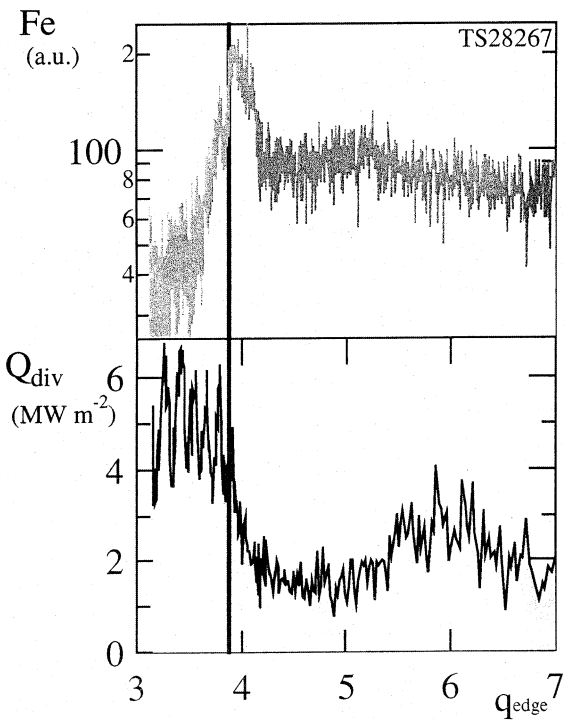

Fig. 2. Transition from limiter to divertor configuration as q_{edge} is decreased, top curve for iron emission, lower curve for parallel energy flux to the divertor.

q_{edge} further decreases to the flat top value, there is no evidence of a weakening of either the energy flux to the target plate or of the iron screening capability, although the radial extent of the divertor volume decreases, Fig. 1. In fact, it can be shown that the mean value of the Chirikov parameter in the divertor volume exhibits a maximum at $q_{edge} \sim 3$, the value of the so-called resonance of the ergodic divertor [1]. The experimental investigation of the geometry of the stochastic boundary thus validates the predicted location of the separatrix [9]. Furthermore, it shows that the plasma response to such a boundary is more complex than would stem from a purely geometrical effect [9].

3. Control of particle recirculation

Particle recirculation is controlled either by increasing the plasma screening capability or by changing the effective extent of the stochastic boundary. In the latter case, four different procedures have been investigated [6,10]: (a) by varying the magnitude of the divertor perturbation monitored by the divertor current I_{ED}; (b) by varying q_{edge}, see Fig. 1; (c) by introducing the outboard pump limiter ahead of the divertor so that recycling on this component will occur much closer to the separatrix; (d) by using helium as working gas since its ionisation mean free path is different from that of deuterium.

Atomic processes that contribute to divertor physics depend strongly on plasma temperature, so that divertor states can only be compared at a given temperature [11]. Most of the experiments have thus been carried out with gas injection feedback on T_{div}, the divertor temperature measured by Langmuir probes [12]. The balance between the neutral outflux, measured with the 2-D image of the Hα line emission, and the ion outflux, measured by the Langmuir probe saturation current multiplied by the computed value of the wetted surface [13], indicates that particle channelling to the target plate is effective, Fig. 3. The divertor temperature is thus a relevant parameter to control the divertor state [11]. Furthermore, extending the analysis to the whole wetted surface indicates that the gas injection rate required in the feedback process amounts to less than 4% of the recycling particle flux [13].

It is convenient to use the divertor tightness $\text{Tight} = n_{div}/\langle n_e \rangle$ as a figure of merit for the control of particle recirculation. Without core fuelling, strong control of particle recirculation will lower the core density $\langle n_e \rangle$, leading to large values of Tight. The relationship between core and divertor densities is computed with a 0-D particle flux balance. Let $\Gamma_{div} S_{div} \exp(-\Delta/\lambda_I)$ be the core influx, S_{div} being the total wetted surface, Γ_{div} the average ion outflux, Δ the radial extent of the screening region with vanishing confinement time and λ_I the ionisation mean free path. This flux must balance the core plasma outflux $\langle n_e \rangle V/\tau_p$. V is the plasma volume

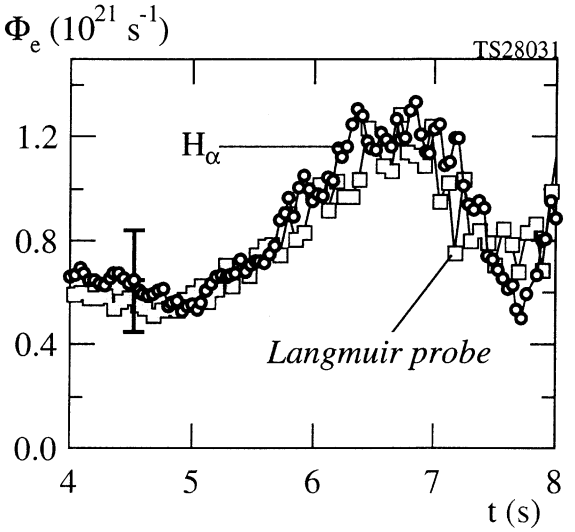

Fig. 3. Time trace of the total particle flux on one out of the 42 target plates of the Tore Supra ergodic divertor. Particle flux computed from the Hα signal is measured with a 2-D image of the target plate. The Langmuir probe data is multiplied by the wetted surface of the target plate, 8×10^{-2} m^2.

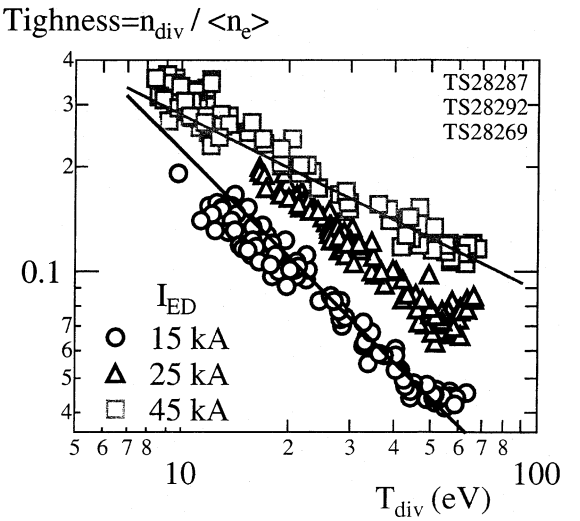

Fig. 4. Tightness of the ergodic divertor plotted against the divertor temperature T_{div}. Results of this temperature scan are presented for three values of the divertor perturbation; maximum perturbation at 45 kA.

and τ_p the core particle confinement time. For a given energy flux to the target plate one finds

$$\text{Tight} = \frac{n_{div}}{\langle n_e \rangle} = \frac{V}{S_{div} c_s \tau_p} \exp\left(\frac{\Delta}{\lambda_I}\right). \quad (1)$$

At given τ_p and screening efficiency, Tight exhibits a $T_{div}^{-0.5}$ dependence due to the sound velocity c_s. Such a scaling appears to fit data at maximum perturbation current, Fig. 4. However, allowing for τ_p to scale like τ_E and using the ITER96's [14] scaling law for L-mode confinement leads to the scaling

$$\text{Tight} \propto \frac{Q_{div}^{0.55} T_{div}^{0.17}}{(1 - f_R)^{1.22} I_p^{1.6}} \exp\left(\frac{\Delta}{0.6\lambda_I}\right). \quad (2)$$

Since Q_{div}, the parallel energy flux to the target plate, and f_R, the radiated fraction, remain roughly constant for $T_{div} \geqslant 15$ eV, the observed dependence on T_{div} must be governed by the exponential screening term. In such a regime ($Q_{div} \sim$ constant), T_{div} also determines n_{div}. The variation of the achieved core density, Fig. 5, with the radial extent of the divertor (I_{ED}) is governed by Δ in the screening factor. The reduction in core density going from a weak divertor perturbation, Fig. 5, to maximum perturbation is typically of 10^{19} m^{-3} for the whole range of T_{div}. The screening capability of the divertor thus impacts directly on the core performance. Such an effect can only be balanced by core particle fuelling, namely pellet injection.

At given divertor parameters, it can be seen that Tight exhibits a linear increase with I_{ED}, Fig. 6. Such a linear dependence is characteristic of laminar transport [1]. The factor 2 increase of Tight, from $I_{ED} \sim 15$ to 45 kA, indicates that the variation in the screening factor is weak so that $\Delta \sim \lambda_I$ at $I_{ED} \sim 15$ kA. A fit of the core density $\langle n_e \rangle$ as a function of I_{ED} for $T_{div} \sim 10$ eV, indicates that two particle sources should be considered: a fast neutral population that accounts for 20–40% of the core fuelling at $I_{ED} \sim 15$ kA, and a slower population

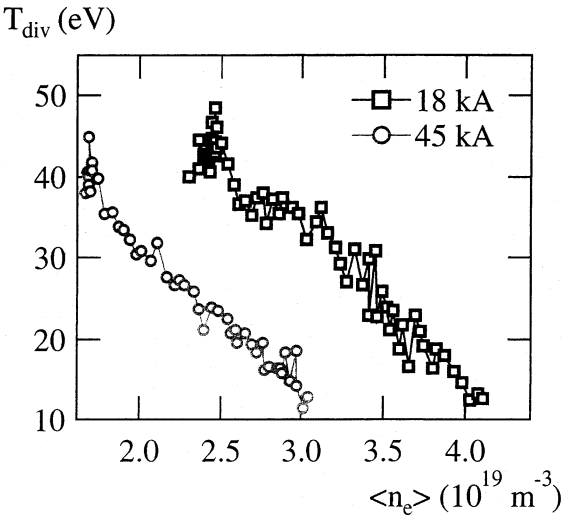

Fig. 5. Divertor temperature T_{div} plotted versus the volume averaged core density $\langle n_e \rangle$ for two values of the divertor perturbation. Note the significant decrease of core density at maximum perturbation.

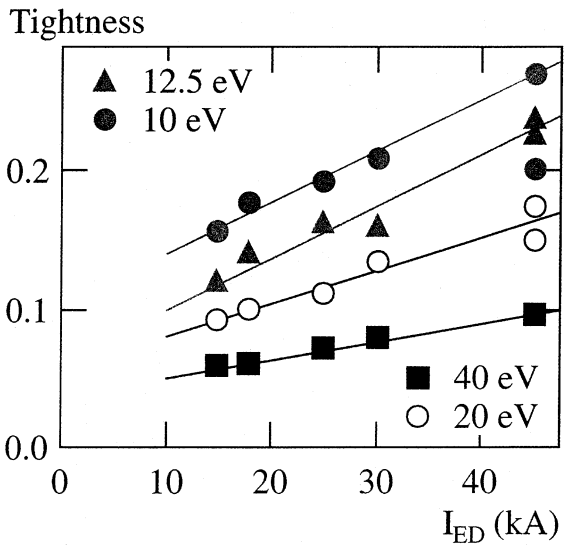

Fig. 6. Divertor tightness versus the magnitude of the divertor perturbation for various values of the divertor temperature.

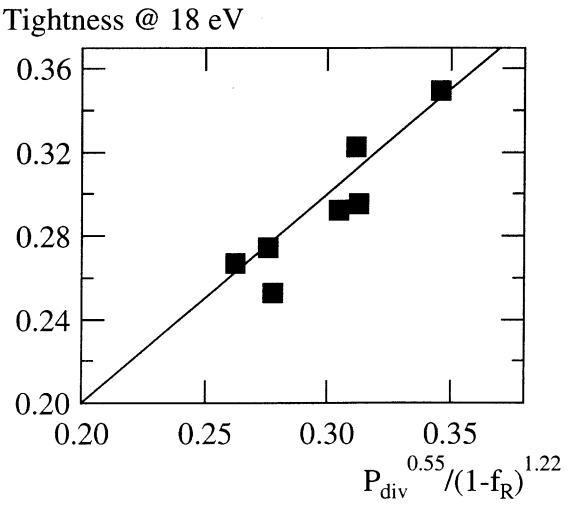

Fig. 7. Divertor tightness at given divertor temperature versus the scaling in terms of the power balance; P_{div} is the power to the target plate and f_R the radiated fraction.

that is gradually screened as the divertor perturbation is increased, 50% of the latter population being screened out at $I_{ED} \sim 45$ kA. Reasonable agreement is found when the slow and fast neutral fluxes are comparable with slow neutrals at ~2.5 eV, fast neutrals at ~22 eV [15], and a density e-folding length of ~0.04 m [13]. This analysis thus indicates that the radial extent of the low particle confinement region is typically of ~0.065–0.07 m at 45 kA with 0.06 m due to the field deflection [1] and less than ~0.01 m due to cross-field transport [13].

As also noticeable in Fig. 6, tightness increases as the divertor temperature is reduced, and hence as the edge density increases. Strong decrease of the ionisation cross-section, and thus decrease of the screening efficiency bounds this effect to $T_{div} \sim 10$ eV. Control of particle recirculation in open configurations is thus very sensitive to the plasma state. A means to further increase the boundary density while avoiding detachment is to operate with additional heating. This has allowed for a moderate increase of the divertor tightness [6], in agreement with the scaling of Eq. (2), Fig. 7. A further benefit of the increased energy flux due to additional heating is the increase in core density. This improves the core performance while enforcing the divertor tightness [6].

Control of particle recirculation is important with respect to both pumping, and especially the key issue of He-ash control, as well as impurity influx control. Dedicated companion papers address these points, achievements of pumping with vented target plates [10], carbon emission and transport in the vicinity of the target plates [16] and neon compression [17].

4. Control of power deposition

An outstanding issue in evaluating divertor performances is the ability to lower the power deposition on the target plates in order to meet the technological constraints of actively cooled components. Operation with the actively cooled target plates of the ergodic divertor on Tore Supra has only met this limitation during lower hybrid acceleration of a beam of electrons at the very location of the target plates [5]. Routine operation leads to a perpendicular energy flux in the 0.7 MW m^{-2} range, (~5 MW m^{-2} in the parallel direction) more than a factor of 10 below the design limit [5]. Experiments with extrinsic impurity injection have been performed in order to further lower the energy flux to the target plates, [7]. Making use of the opportunity of working at given divertor plasma temperature, nitrogen injection experiments have been revisited since this impurity allows one to increase the radiation capability at optimum divertor temperature, $T_{div} \sim 10$ eV, despite the sharp decrease of the intrinsic carbon flux [16,18]. Data for nitrogen injection are compared to standard impurities used in radiative divertor experiments, namely neon and argon.

A figure of merit of divertor radiation capability is the achieved reduction in energy flux to the target plate and its cost in terms of core dilution, usually characterised by the plasma effective charge, Z_{eff}. To illustrate this divertor performance, the contribution of the injected impurities to Z_{eff}, ΔZ_{eff}, is plotted against the parallel energy flux to the target plate, Fig. 8. The latter parameter is the relevant one for radiative divertor performance. Furthermore, Langmuir probe data and

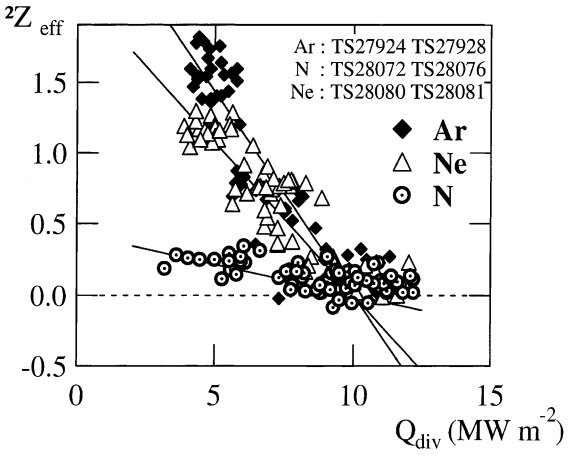

Fig. 8. Contribution to Z_{eff} of the injected impurities versus the parallel energy flux to the divertor Q_{div}. Optimised impurity injection leads to the lowest value of Q_{div} and the lowest contribution to Z_{eff}, $\Delta Z_{eff} \sim 0$.

IR camera measurements are in good agreement [19], while toroidal dependence of radiation leads to systematic errors in the radiative power measurement with the bolometer cameras [20]. It is clear from this experimental evidence that the use of the appropriate impurity for divertor radiation leads to the best results, both the lowest parallel heat flux, and the lowest contribution to Z_{eff}. On the other hand, Ne and Ar injection also lead to a significant reduction of the energy flux to the target plate but at the cost of a large contribution to Z_{eff}. The strongest radiation enhancement with the ergodic divertor [5] is therefore achieved with nitrogen injection. Let us now consider the core dilution required for a drop of 10 MW m^{-2} of the parallel heat flux. Using the data of Fig. 8, one finds that the nitrogen, argon and neon contribution to the electron density would then reach, respectively, 7%, 16% and 23%. The low performance of neon injection experiments, despite the observed neon compression in the divertor volume [17], is governed by the plasma temperature required to reach strong radiation rates. In order to analyse this effect, radiation compression has been computed from experimental data and 1-D modelling of divertor radiation [7]. Radiation compression is the ratio of the radiating impurity concentration in the divertor to the core impurity concentration. This figure of merit is comparable to the ratio of divertor radiation to core radiation, the latter being characterised by the multi-machine scaling proportional to $(Z_{eff} - 1)$ [3]. It is then found that Ne and Ar exhibit comparable and small radiation compression, typically $\sim$2, while N reaches much higher values, from 8 to 10. Intermediate values, $\sim$5, are reported for the intrinsic impurities, mainly carbon at low density, together with oxygen and chlorine at varying concentrations at higher densities [7].

Theoretical investigation of radiation in the 3-D temperature field indicates that the plasma temperature is not monotonic along field lines, in contrast to profiles expected in the axisymmetric divertor. The temperature variation, and in particular the change in parallel gradient, is directly related to the radial excursion of the field lines and the temperature equilibration of a given field line with the background due to cross-field transport. Temperature drop and density condensation can then occur at the same location leading to a radiating structure with small 'Marfes' [21] distributed in the divertor volume. Cross-field transport is also a key element to transfer energy to these localised sinks. The increase of density fluctuation at large densities [22] would then provide an alternative energy transport when parallel energy transport collapses at low temperature [20].

5. Conclusion

Ten years of operation of the ergodic divertor on Tore Supra have allowed remarkable achievements. It is shown that core performances are not affected in this configuration and in particular that neither the plasma current nor the energy confinement are changed when the outer 36% of the volume of closed field lines are changed into a volume of open field lines. Unlike the axisymmetric divertor, the ergodic divertor does not require an edge transport barrier to recover the performance level achieved when using the whole magnetised volume.

Regarding the control of plasma surface interaction, the latest experimental evidence from the final campaign in 1999, enforces previous results. Particle control with channelling of the particle flux to the vented target plate, as well as the strong ionisation of the recycling particle flux within the divertor volume, the so-called tightness, are shown to be effective. This effect appears to scale like the laminar transport and is therefore sensitive to the geometry of the magnetic field perturbation. This leaves some flexibility for further optimisation of pumping with the vented target plates.

Finally, radiation compression within the divertor volume as well as impurity control provide a means to achieve very low energy fluxes to the target plates, typically a factor of 10 below standard SOL values. It is remarkable that nearly all the parallel energy flux recorded in the experiments could be removed with the ergodic divertor components orthogonal to field lines. In practise, such a magnitude of incident energy flux has been achieved locally on leading edges of the target plates due to shortfalls in the design of the vented structure.

The future of the ergodic divertor concept exhibits three characteristic time scales. In the near future, the Textor DED will come into operation [23]. A future

ergodic divertor is possible on Tore Supra provided a large amount of power is available to maximise the divertor tightness. Operation in conjunction with internal transport barriers would be valuable. Extrapolation of the concept to nuclear grade machines has been analysed and in particular it has been shown that reasonable octopolar perturbations of the plasma could still be sustained with superconducting coils behind 1 m thick neutron shields [24].

References

[1] Ph. Ghendrih, A. Grosman, H. Capes, Plasma Phys. Control. Fus. 38 (1996) 1653.
[2] Ph. Ghendrih, A. Grosman, J. Gunn, F. Laugier, B. Meslin et al., J. Nucl. Mater. 266–269 (1999) 189.
[3] K. Behringer, A. Boileau, F. Bombarda, G.B. Denne, W. Endelhardt et al., in: Proceedings of the 11th IAEA International Conference, Kyoto, 1986, in: Plasma Physics and Controlled Nuclear Fusion Research, vol. 1, IAEA, Vienna, 1987, p. 197.
[4] G.F. Matthews, S. Allen, N. Asakura, J. Goetz, H. Guo et al., J. Nucl. Mater. 241–243 (1997) 450.
[5] Ph. Ghendrih, Plasma Phys. Control. Fus. 39 (1997) B207.
[6] C. Grisolia et al., these Proceedings.
[7] P. Monier-Garbet et al., these Proceedings.
[8] K. Kaufmann, H.-S. Bosch, A. Hermann, A. Kallenbach, K. Borrass et al., in: Proceedings of the 18th IAEA Conference on Fusion Energy, Yokohama, Japan, in: Fusion Energy 1998, vol. 1, IAEA, Vienna, 1999, p. 317.
[9] M. Zabiégo et al., these Proceedings.
[10] T. Loarer et al., these Proceedings.
[11] I.H. Hutchinson, G.C. Vlases, Nucl. Fus. 36 (1996) 783.
[12] J. Bucalossi et al., these Proceedings.
[13] J. Gunn et al., these Proceedings.
[14] S.M. Kaye, ITER Confinement Database Working Group, Nucl. Fus. 37 (1997) 1303.
[15] A. Escarguel et al., these Proceedings.
[16] Y. Corre et al., these Proceedings.
[17] R. Guirlet et al., these Proceedings.
[18] B. Schunke et al., these Proceedings.
[19] L. Costanzo et al., these Proceedings.
[20] F. Laugier et al., these Proceedings.
[21] B. Lipschultz, J. Nucl. Mater. 145–147 (1987) 15.
[22] P. Devynck et al., these Proceedings.
[23] G. Mank et al., these Proceedings.
[24] A. Azéroual, J.-M. Ané, X. Chen, Ph. Ghendrih, V. Grandgirard, A. Grosman, B. Pégourié, in: B. Beaumont, P. Libeyre, B. de Gentile, G. Tonon (Eds.), Proceedings of the 20th SOFT, Fusion Technology 1998, St Paul lez Durance, 1998, p. 1705.